

## Research Article

# Single Remote Sensing Multispectral Image Dehazing Based on a Learning Framework

Shuai Shao <sup>1,2</sup>, Yongfei Guo,<sup>1</sup> Zeshu Zhang,<sup>1</sup> and Hangfei Yuan<sup>1</sup>

<sup>1</sup>Changchun Institute of Optics, Fine Mechanics and Physics, Chinese Academy of Sciences, Changchun 130033, China

<sup>2</sup>University of Chinese Academy of Sciences, Beijing 100049, China

Correspondence should be addressed to Shuai Shao; damond0424@yeah.net

Received 4 July 2018; Revised 2 December 2018; Accepted 10 December 2018; Published 3 January 2019

Academic Editor: Erik Cuevas

Copyright © 2019 Shuai Shao et al. This is an open access article distributed under the Creative Commons Attribution License, which permits unrestricted use, distribution, and reproduction in any medium, provided the original work is properly cited.

Given that a single remote sensing image dehazing is an ill-posed problem, this is still a challenging task. In order to improve the visibility of a single hazy remote sensing multispectral image, we developed a novel and effective algorithm based on a learning framework. A linear regression model with the relevant features of haze was established. And the gradient descent method is applied to the learning model. Then a hazy image accurate transmission map is obtained by learning the coefficients of the linear model. In addition, we proposed a more effective method to estimate the atmospheric light, which can restrain the influence of highlight areas on the atmospheric light acquisition. Compared with the traditional haze removal methods, the experimental results demonstrate that the proposed algorithm can achieve better visual effect and color fidelity. Both subjective evaluation and objective assessments indicate that the proposed method achieves a better performance than the state-of-the-art methods.

## 1. Introduction

Remote sensing images are widely applied to various fields because of its high spatial resolution and stable geometric location [1–3]. However, the process of remote sensing images acquisition is vulnerable to the atmospheric conditions (e.g., hazy or foggy), resulting from the fact that light is absorbed and scattered by the turbid medium such as particles and water droplets in the atmosphere [4–6]. Consequently, the technique of haze removal has received more attention in improving the visibility of satellite imagery. Nevertheless, how to achieve a single remote sensing image haze removal is still a challenging task since the regions spoiled by haze contain both ground features and haze components.

In the past decades, along with the development of computer and computer vision, the investigations on haze removal for satellite imagery have got some progresses. Chavez *et al.* [7, 8] improved dark-object subtraction (DOS) method to correct optical data for atmospheric scattering. This method assumes that the reflectivity of the pixels is very low, but, owing to the existence of haze, the number (DN) in these pixels is nonzero. Therefore, the values of the DN can be taken as the haze thickness. Then the DN value is

subtracted from a hazy image to achieve haze removal. Based on the researches by Chavez, Makarau *et al.* [9] searched for dark objects locally in the whole image to construct a haze thickness map (HTM). Therefore, subtracting the HTM from a hazy image leads to haze removal. Zhang *et al.* [10] proposed a haze optimized transformation (HOT) algorithm, to achieve haze region removal based on analyzing the features of visible-band space. But this method is not suitable for bright surfaces. Ni *et al.* [11] developed a method based on using linear intensity transformation (LIT) and local property analysis (LPA). However, this method strongly depends on the accurate estimation of LIT and LPA for haze removal.

Recently, the processing of single hazy image has a significant progress. Some methods based on polarization have been developed. Schechner *et al.* [12] created a scene's distance map by utilizing the fact that one of the sources of image degradation in haze is partially polarized. Wang *et al.* [13] proposed a single image dehazing method based on adaptive wavelet fusion, which could preserve the most discriminant scene depth. Liu *et al.* [14] developed a polarization dehazing method by processing the low spatial frequency parts and the high spatial frequency parts separately. Regarding the

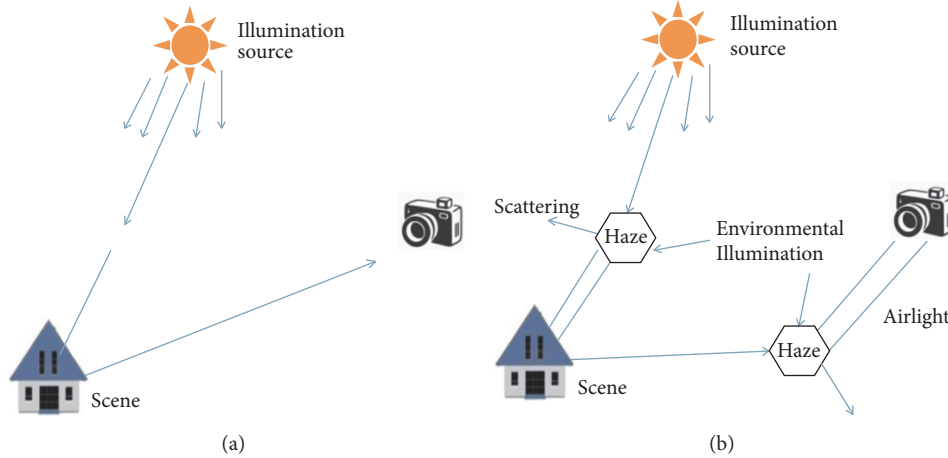


FIGURE 1: The atmosphere scattering model for different weather conditions. (a) Sunny weather. (b) Hazy weather.

image fusion method, Li *et al.* [15] proposed a single image dehazing approach based on a multiscale pyramid fusion scheme. In addition, with the development of deep learning, some researchers employed convolutional neural networks for single hazy image processing. Ren *et al.* [16] created a multiscale convolutional neural network model to learn the transmission map. After that, Li *et al.* [17] present a truly end-to-end network, combining the transmission map with the atmospheric light to produce the results. Nevertheless, these methods are complex and time consuming. Tang *et al.* [18] analyzed four types of haze relevant features and utilized Random Forests to learn the transmission map. Jiang *et al.* [19] proposed a method for gray-scale image dehazing, but it was not suitable for inhomogeneous scenes. Gu *et al.* [20] developed a dehazing method based on average saturation prior, which improved the atmospheric scattering model to cope with the inhomogeneous atmospheric light.

Some single image dehazing methods based on the physical model also have been promoted. Tan *et al.* [21] firstly proposed a single image dehazing method by maximizing the local contrast of the image. Although Tan's approach is able to produce color over saturation with images with dense haze, Fattal *et al.* [22] removed the haze from color images based on Independent Component Analysis (ICA), but the approach is not suitable for the gray scale image haze removal. He *et al.* [23] summarized a rule that was called dark channel prior (DCP) based on observing the statistical characteristics pertaining to a large number of hazy free images. Then the real scene radiance is recovered based on DCP. Among the above methods, He's method is simple and effective. However, the DCP method is based on the statistics of the outdoor hazy images, while remote sensing images have a different imaging distance with the outdoor images. As a result, the color drift is easily caused when applied to the remote sensing image.

In this paper, we proposed a novel haze removal method for single remote sensing images. By analyzing the haze relevant features (including luminance component, saturation component, and saliency component), we have established a linear regression model with multiple variables. The

correlation between the hazy image and its corresponding transmission map is detected effectively based on learning the coefficients of the linear model. In addition, the atmospheric light was estimated by an improved method, which can reduce the influence of highlight areas on the atmospheric light acquisition. With the recovered transmission information and the estimation of the atmospheric light, the haze-free image can be recovered. Compared with the traditional haze removal technology on remote sensing images, the algorithm can achieve better results.

The remainder of this paper is organized as follows. Section 2 provides the details of our method, including physical hazy image degradation model, atmospheric light estimation, and linear regression model training. The experimental results are listed in Section 3; we present both subjective evaluation and objective assessments. Finally, conclusion is present in Section 4

## 2. Proposed Method

*2.1. The Physical Hazy Image Degradation Model.* Nayer and Narasimhan [24, 25] have a detailed description and derivation of the atmospheric scattering model, as shown in Figure 1, and the model is widely referenced by later researchers. They divide the influence of the light reflected by the atmosphere into two parts: direct attenuation and veiling light. The formation of a hazy image can be described as

$$\mathbf{I}(x) = \mathbf{J}(x)t(x) + \mathbf{A}(1 - t(x)) \quad (1)$$

where  $x$  represents the position of the pixel in the image,  $\mathbf{I}(x)$  is the observed hazy image,  $\mathbf{J}(x)$  is the scene radiance,  $\mathbf{A}$  is the global atmospheric light usually assumed to be constant, and  $t(x)$  is the medium transmission, which describes the ratio of the light that is not scattered and gets to the camera. The medium transmission can be expressed as

$$t(x) = e^{\beta d(x)} \quad (2)$$

where  $d(x)$  is the scene depth and  $\beta$  is the scattering coefficient of the atmosphere. The goal of dehazing is to

estimate the  $(x)$ ; we can obtain the real scene  $\mathbf{J}(x)$  since we have an estimate of  $\mathbf{A}$  and  $t(x)$  by

$$\mathbf{J}(x) = \frac{\mathbf{I}(x) - \mathbf{A}}{t(x)} + \mathbf{A} \quad (3)$$

**2.2. Estimation of the Atmospheric Light.** Most of the haze removal algorithms are based on the pixels associated with a single image to obtain an estimation of the atmospheric light. When the step of remote sensing image acquisition is under the condition of hazy weather, we commonly ignore the influence of sunlight. Tan *et al.* [21] utilized the maximum value of the pixels in the hazy image as estimation of atmospheric light, while the maximum values of the luminance component may belong to the highlighted object regions. In He's work [23], the top 0.1% pixels in dark channel are taken as the atmospheric light. Although this method is robust, only taking one point into account may cause that the  $\mathbf{A}$  value of each channel is too high to lead to color drift. Conventional ways tend to be hard to achieve a satisfactory result when the highlight areas exist in image.

Based on the work of He and others, we developed a method that can reduce the influence of highlight areas on the atmospheric light acquisition. First of all, it is required to take the minimum channel map of the degraded remote sensing images. The minimum channel map is calculated as

$$M(x) = \min_{c \in (r, g, b)} (I_c(x)) \quad (4)$$

Based on the weighted quad-tree search method [23], the minimum channel map of the hazy image is divided into four average areas by location and then the score of each region is obtained:

$$score_i = \overline{M}_i - \delta_i^2, \quad i = 1, 2, 3, 4 \quad (5)$$

where  $i$  is the index of each region,  $score_i$  is the score of region  $i$ ,  $\overline{M}_i$  represents the mean value of the region  $i$ , and  $\delta_i^2$  represents variance in the region  $i$ . Then take the region with the highest score as the candidate iterative region, and it is further divided into four smaller regions. This process continues to iterate until the size of the candidate region is smaller than the preset size threshold. The average of each channel in the last candidate region is selected as the result of  $\mathbf{A}$ .

**2.3. Transmission Estimation.** According to eq. (1), we can recover the real scene if we have acquired the estimation of atmospheric light and the transmission map. Thick haze can cause high brightness, flatness, and unsaturation in the image. We developed a linear regression model to estimate the haze concentration based on investigating various haze relevant features. Saliency represents which regions stand out from the neighbors and are the most attractive [26]. Due to the influence of haze, a large amount of information (color, edge, etc.) in the image is damaged, and the saliency of the target is also greatly affected. So the luminance component  $I_L$ , the saliency component  $S_a$ , and the saturation component  $I_s$  have

a strong relationship with the distribution of haze [15, 26, 27]. The concentration of haze  $F(x, y)$  is described as follows:

$$F(x, y) = \theta_0 + \theta_1 I_L(x, y) + \theta_2 I_s(x, y) + \theta_3 S_a(x, y) \quad (6)$$

where  $\theta_i$ ,  $i \in (0, 1, 2, 3)$ , represents the nonnegative coefficients of the linear regression model with multiple variables in eq. (6). As a result of transmission is inversely proportional to the haze density, a linear model between transmission and the haze concentration feature was developed as follows:

$$t(x, y) = 1 - \beta F(x, y) \quad (7)$$

where  $\beta$  is a nonnegative coefficient; for computational and description convenience, we rewrite Eq. (6) as

$$F_\theta(X) = \theta_0 X_0 + \theta_1 X_1 + \theta_2 X_2 + \theta_3 X_3 \quad (8)$$

where  $X_0 = 1$ ,  $X_1 = I_L(x, y)$ ,  $X_2 = I_s(x, y)$ ,  $X_3 = S_a(x, y)$ . The gradient descent method is applied to learn  $\theta_i$  and a cost function  $J(\theta_i)$ , which is the sum of squares of all modeling errors; the cost function can be described as

$$J(\theta) = \frac{1}{2m} \sum_{i=1}^m (F_\theta(X^i) - y^i)^2 \quad (9)$$

where  $m$  represents the total number of training samples and  $y^i$  indicates the actual value of the sample. Then, by minimizing the cost function, we can obtain the series of coefficients. At the beginning, we randomly select a combination of parameters  $(\theta_0, \theta_1, \theta_2, \theta_3)$  to calculate the cost function. Then we traced the next combination of parameters to ensure that the value is reduced at the most rapid rate. Continue to do the above steps until the cost function reaches a local minimum. The derivative of the cost function is calculated as follows:

$$\frac{\partial}{\partial \theta_j} J(\theta) = \frac{\partial}{\partial \theta_j} - \frac{1}{2m} \sum_{i=1}^m (F_\theta(X^i) - y^i)^2 \quad (10)$$

And according to the gradient descent algorithm we have

$$\theta_j := \theta_j - \alpha \frac{\partial}{\partial \theta_j} J(\theta) \quad (11)$$

In the gradient descent algorithm,  $\theta$  is updated during gradient descent. Then we can acquire the following expression:

$$\theta_0 := \theta_0 - \alpha \frac{1}{m} \sum_{i=1}^m (F_\theta(X^i) - y^i) \quad (12)$$

$$\theta_1 := \theta_1 - \alpha \frac{1}{m} \sum_{i=1}^m F_\theta((X^i) - y^i) X_1^{(i)} \quad (13)$$

$$\theta_2 := \theta_2 - \alpha \frac{1}{m} \sum_{i=1}^m F_\theta((X^i) - y^i) X_2^{(i)} \quad (14)$$

$$\theta_3 := \theta_3 - \alpha \frac{1}{m} \sum_{i=1}^m F_\theta((X^i) - y^i) X_3^{(i)} \quad (15)$$

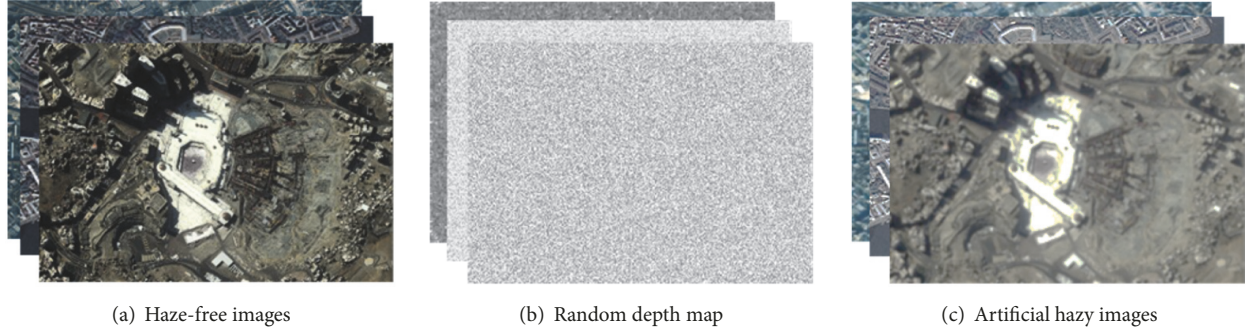


FIGURE 2: The procedure of building training samples.

where the notation  $:=$  represents setting the value  $\theta_j$  in the left side of the equation to be the value of the right side and  $\alpha$  is the learning rate, which determines the efficiency of the gradient descent algorithm. If learning rate is too small, we would need a large number of steps to reach the global minimum. Conversely, the cost function is unable to converge when learning rate is too large. Thus, it is significant to choose the right learning rate, and the calculation of the learning rate is shown as follows:

$$\alpha = \alpha_s * \alpha_D^{(global-step)/(decay-step)} \quad (16)$$

where  $\alpha_s$  is initial learning rate,  $\alpha_D$  indicates the attenuation rate of each round of learning,  $global - step$  represents the current number of learning steps which is equivalent to how many times we put batch into the learner, and  $decay - step$  is the number of steps per round of learning which is equal to the total number of samples divided by the size of each batch.

**2.4. Training Data Preparation.** In order to learn the coefficients in eq. (6) accurately, we prepared the training data based on the method proposed by Tang et al. [18]. Tang assumed that the image content is independent of scene depth or media transmission, and depth is locally constant. We illustrated the procedure of generating the training data in Figure 2. At first, we generated a random depth map with equal size for each unblemished image, and the pixel values in the synthetic depth map were extracted from the standard uniform distribution in the open interval (0, 1). Then we generated random atmospheric light  $A$  ( $m, m, m$ ), where  $m$  is between 0.8 and 1. Finally, according to equation (1) and equation (2), we can obtain the hazy image  $I$  by utilizing the random depth map  $d$  and the random atmospheric light  $A$ . For transmission to be revealed better, we randomly collect 600 haze-free remote sensing images from the Google Earth for generating the training data. The procedure of preparing training samples is shown in Figure 2. The best learning result is that  $\theta_0 = 0.1217$ ,  $\theta_1 = 0.9571$ ,  $\theta_2 = 0.7806$ ,  $\theta_3 = -0.54138$ ,  $\beta = 0.82178$ . Due to the fact that acquisition of these coefficients is based on the statistical characteristics of the training data, these coefficients ultimately represent the common characteristics of remote sensing hazy images. Through a large number of experiments on the real remote sensing hazy images, we found that these coefficients can be

applied for a single remote sensing image to achieve thin haze removal and obtained good results. And we will give a discussion of the experiments in Section 3.

**2.5. Scene Radiance Restoration.** Since the transmission map and the atmospheric light were known, the scene radiance can be recovered according to (1). However, the direct attenuation term  $J(x)t(x)$  can be very close to zero when the transmission  $t(x)$  is close to zero. That will bring a lot of noise. Inspired by Zhu et al.'s method [27], we restrict the transmission to an extent. Thus, the scene radiance restoration can be expressed as

$$J(x) = \frac{I(x) - A}{\min\{\max\{t(x), 0.1\}, 0.9\}} + A \quad (17)$$

### 3. Experiments and Evaluation

In this section, in order to verify the effectiveness of the method, multiple hazy visible images of several satellites data were tested. The performance of the proposed method is compared with DCP [23], HOT [10], Qin et al.'s [3], Liu et al.'s [4], and Multiscale Retinex [28] methods both qualitatively and quantitatively. All the experiments are carried out on the MatlabR2014a environment with a 2.5GHz PC and 4GB RAM.

**3.1. Subjective and Comparative Evaluation.** The transmission map results are compared between He's original dark channel prior [23] results and our algorithm, as shown in Figure 3. As we can see, the transmission map obtained in this paper can capture sharp edge discontinuity points and outline the outline of the object, and halo and block artifacts have been effectively suppressed.

As shown in Figure 4, these hazy images data are collected from Google Earth and NASA Earth Observatory website. Figure 4(a) represents the input hazy images with uniform haze. Figure 4(b) represents the results of Multiscale Retinex method, which can achieve the effect of haze removal. But when the original image does not satisfy the gray-scale assumption, it will lead to color distortion. Figure 4(c) is the DCP method results; constrained by the inherent problem of dark channel priors, He's algorithm cannot be applied to regions where brightness is similar to atmospheric

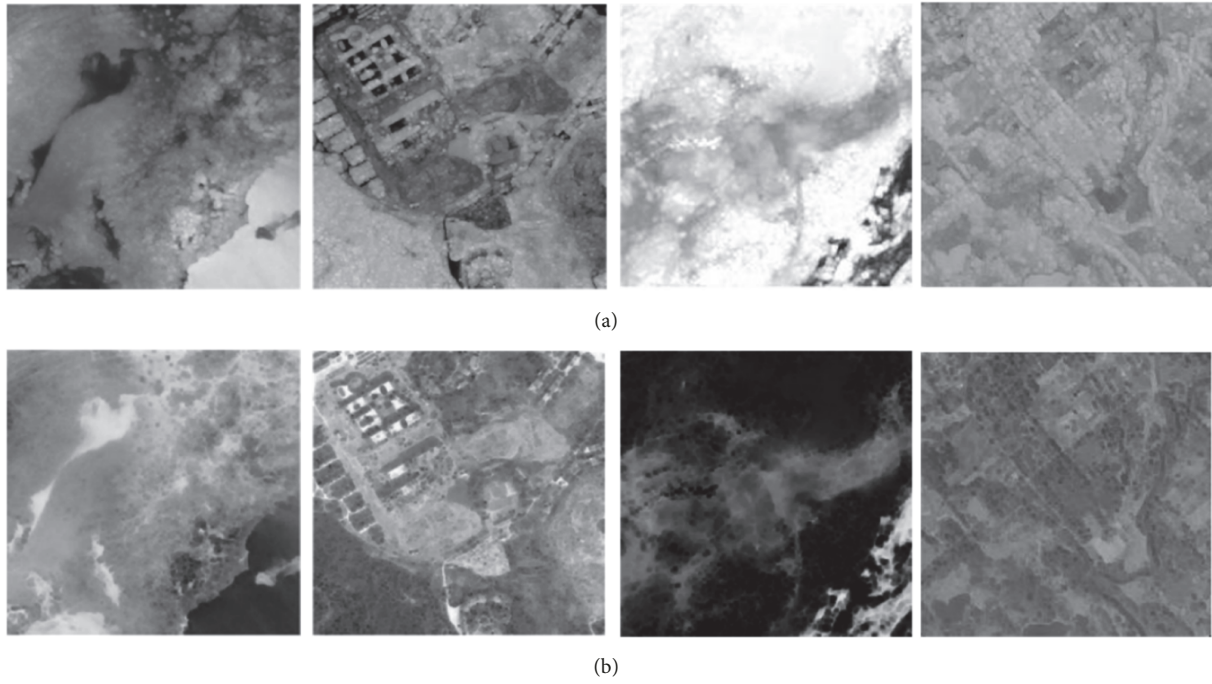


FIGURE 3: The transmission map comparisons. (a) DCP method results. (b) Our results.

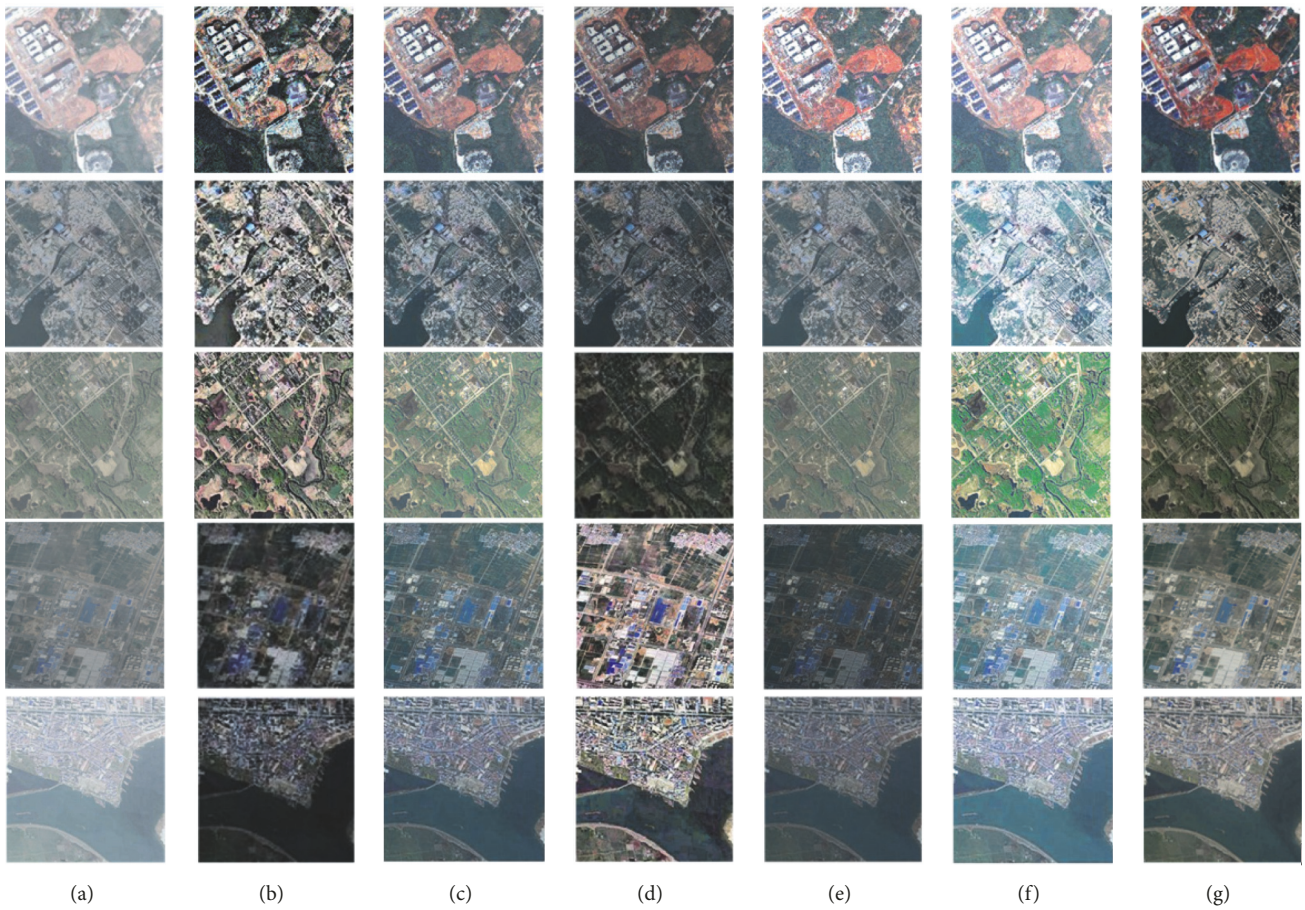


FIGURE 4: Qualitative comparison of different methods in processing images with uniform haze. (a) The hazy images. (b) MSR method results. (c) DCP method results. (d) HOT method results. (e) Qin's method results. (f) Liu's method results. (g) Our results.

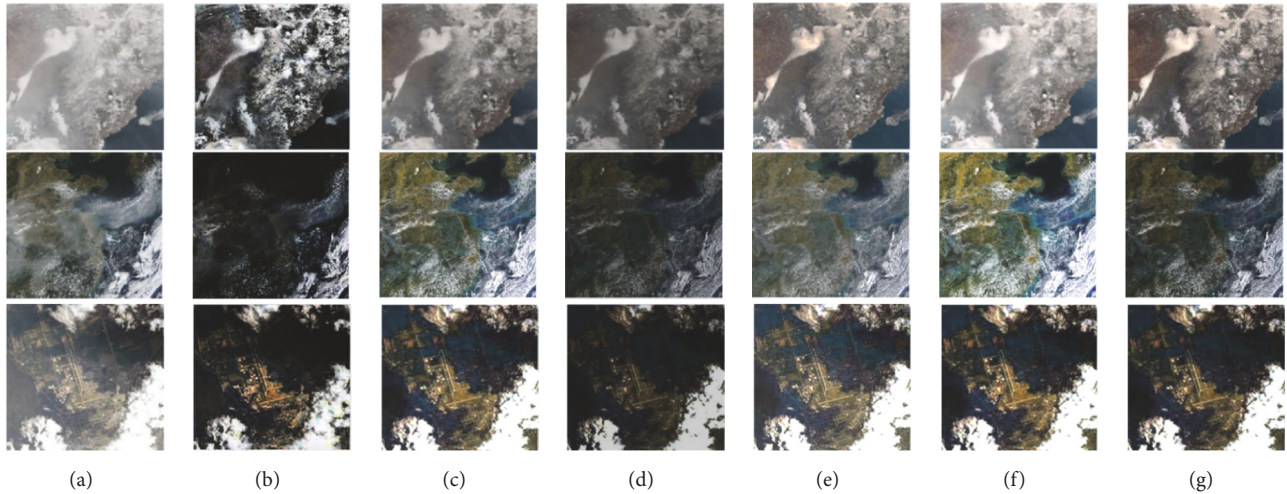


FIGURE 5: Qualitative comparison of different methods in processing images with uneven haze. (a) The hazy images. (b) MSR method results. (c) DCP method results. (d) HOT method results. (e) Qin's method results. (f) Liu's method results. (g) Our results.

light. Therefore, the DCP method is often unreliable when dealing with nonhomogeneous images. Figure 4(d) is the HOT method results; most of hazes have been removed, but the recovered image has a slight color distortion, and the resolution of the image will be lower than that of the original image. By observing the images in Figures 4(e) and 4(f), we can find that the results of Qin's [3] and Liu's [4] are blurred, along with color distortion. Figure 4(g) is our method results; as can be seen, the mist is effectively removed and the color fidelity is preserved well. What is more is that our method achieves a better visual effect.

Figure 5 shows the comparison of dehazing results with the five state-of-the-art dehazing techniques [3, 4, 10, 23, 28] on remote sensing images with uneven haze distribution. To evaluate the availability of this method in dealing with uneven distribution haze, several representative images were selected. Compared with the results of Qin's [3] and Liu's [4], our method achieves better results in removing haze. Similarly, as can be seen from Figures 5(b) and 5(d), MSR [28] results and HOT [10] results have a common phenomenon of color distortion. Figure 5(c) shows He's [23] results; the visual effect of the hazy images has been improved, but the color shift phenomenon still exists in the region with white objects. Furthermore, as shown in Figure 5(g), our algorithm has better performance in terms of haze removal ability, the overall contrast, and color fidelity. Nevertheless, our method is not suitable for thick haze removing.

**3.2. Objective and Comparative Evaluation.** In order to objectively evaluate the algorithms, we select some classical evaluation indexes, including mean squared error (MSE), the ratio of new visible edges ( $e$ ), the gain of visibility level  $\bar{r}$ , the structural similarity (SSIM), the peak signal to noise ratio (PSNR), and the fog aware density evaluator (FADE). The MSE value can be utilized as a more convenient way to evaluate the degree of data variation [29]; a high value of MSE indicates that the haze removal algorithm is not effective while a low value of MSE represents that the recovered image

is valuable. The value of  $e$  evaluates the ability of haze removal method to recover the edges which are not visible in a hazy image. The value of  $\bar{r}$  represents the average ratio of gradient specifications before and after dehazing [30]. The high SSIM value indicates that the haze removal image is highly similar to the real image on the ground [27]. PSNR is calculated based on the error of the corresponding pixels, and the larger PSNR value indicates the slighter distortion [31]. Fog Aware Density Evaluator [32] (FADE) is a contrast descriptor which indicates the visibility of a foggy scene through measuring the statistical regularity deviation of hazy images and haze-free images. A low value of FADE implies better performance of visibility enhancement. The values of MSE, SSIM, PSNR,  $e$ ,  $\bar{r}$ , and FADE are listed in Table 1. Four images belonging to Figures 4 and 5 are selected for illustration. To sum up, our method achieves better results of MSE, FADE,  $e$ , SSIM, PSNR, and  $\bar{r}$ . Therefore, the results of these experimental data indicate that our algorithm achieves better performance on contrast enhancement, visible edge enhancement, and haze removal.

When the linear coefficients are obtained, we display the time consumption comparison with DCP [23], HOT [10], Qin *et al.*'s [3], Liu *et al.*'s [4], and Multiscale Retinex [28] methods. As shown in Table 2, our research is faster than others.

## 4. Conclusion

In this paper, a novel and effective dehazing algorithm was developed to achieve single remote sensing image haze removal. A linear regression model with multiple variables is established and the gradient descent method is applied to the coefficients of the linear model. Then a hazy image accurate transmission map is obtained. In addition, we proposed a more valid method to estimate the atmospheric light, which can restrain the influence of highlight areas. Compared with the traditional methods, the experimental results demonstrate that the developed algorithm has a good performance

TABLE 1: The corresponding values of MSE, SSIM, PSNR,  $e$ ,  $\bar{r}$ , and FADE.

Image	SSIM	$e$	$\bar{r}$	FADE	PSNR	MSE
Original images	0.717	2.517	2.265	0.368	20.15	3.854
	0.695	0.668	2.168	0.706	16.26	4.126
	0.653	1.654	2.463	0.856	18.34	5.021
	0.732	1.786	1.952	0.757	24.32	3.908
MSRCR method	0.754	2.806	1.971	0.269	22.31	3.785
	0.732	0.927	1.932	0.472	19.32	4.103
	0.812	1.781	1.685	0.863	20.08	3.953
	0.795	1.953	1.613	0.617	26.62	3.784
HOT method	0.763	2.763	1.646	0.341	18.31	2.357
	0.742	0.715	2.235	0.620	15.32	2.132
	0.769	1.793	2.361	0.831	16.08	3.416
	0.746	1.851	1.859	0.624	17.62	2.317
DCP method	0.712	2.782	1.836	0.316	21.53	2.365
	0.746	0.757	1.757	0.608	19.56	2.143
	0.812	1.463	2.307	0.741	18.49	3.446
	0.795	1.673	2.135	0.738	25.43	2.512
Qin's method	0.723	2.402	2.158	0.377	23.13	3.613
	0.734	0.745	2.034	0.712	18.31	3.815
	0.681	1.593	2.207	0.796	19.43	4.236
	0.762	1.810	1.604	0.763	24.69	3.752
Liu's method	0.743	2.532	2.242	0.330	21.26	2.854
	0.754	0.716	2.093	0.691	17.57	3.867
	0.703	1.803	2.283	0.637	18.96	4.351
	0.764	1.931	1.759	0.743	23.71	3.648
Ours	0.787	2.794	1.825	0.313	25.13	2.244
	0.795	0.783	1.792	0.496	21.41	2.032
	0.823	1.869	1.785	0.756	24.36	3.132
	0.812	2.103	1.654	0.761	27.28	2.137

TABLE 2: Time consumption comparison with DCP [23], HOT [10], Qin *et al.*'s [3], Liu *et al.*'s [4], and Multiscale Retinex [28] methods.

Image resolution	MSRCR method	DCP method	HOT method	Qin's method	Liu's method	Ours
512×512	9.75s	9.69s	9.31s	9.45s	8.65s	5.42s
1080×720	23.83s	19.36s	20.35s	19.65s	18.56s	9.85s
1280×1080	31.42s	28.67s	32.38s	23.56s	26.78s	14.67s

in thin haze removal and color fidelity remaining. Both subjective evaluation and objective assessments indicate that the proposed method can recover a haze-free remote sensing image with good visual effect and high quality. Furthermore, our future research will turn to the removal of thick haze.

### Data Availability

The data are available from the corresponding author upon request.

### Conflicts of Interest

The authors declare that there are no conflicts of interest regarding the publication of this paper.

### Acknowledgments

This work is partially supported by the National Key R&D Program of China (Grants nos. 2016YFB0500100).

### References

- [1] M. Dalla Mura, J. A. Benediktsson, B. Waske, and L. Bruzzone, "Morphological attribute profiles for the analysis of very high resolution images," *IEEE Transactions on Geoscience and Remote Sensing*, vol. 48, no. 10, pp. 3747–3762, 2010.
- [2] J. Long, Z. Shi, and W. Tang, "Fast haze removal for a single remote sensing image using dark channel prior," in *Proceedings of the 2012 International Conference on Computer Vision in Remote Sensing, CVRS 2012*, pp. 132–135, China, December 2012.
- [3] M. Qin, F. Xie, W. Li, Z. Shi, and H. Zhang, "Dehazing for multispectral remote sensing images based on a convolutional

- neural network with the residual architecture,” *IEEE Journal of Selected Topics in Applied Earth Observations and Remote Sensing*, pp. 1–11, 2018.
- [4] Q. Liu, X. Gao, L. He, and W. Lu, “Haze removal for a single visible remote sensing image,” *Signal Processing*, vol. 137, pp. 33–43, 2017.
- [5] Y. Xiao Chong et al., “Optically sizing single atmospheric particulates with a 10-nm resolution using a strong evanescent field,” *Light Science & Applications*, vol. 7, no. 4, Article ID 18003, 2018.
- [6] W. Yi Chen, “Air quality monitoring using mobile microscopy and machine learning,” *Light Science & Applications*, vol. 6, no. 9, Article ID e17046, 2017.
- [7] P. S. Chavez Jr., “An improved dark-object subtraction technique for atmospheric scattering correction of multispectral data,” *Remote Sensing of Environment*, vol. 24, no. 3, pp. 459–479, 1988.
- [8] P. Chavez, “Image-based atmospheric corrections—Revisited and improved,” *Photogrammetric Engineering and Remote Sensing*, vol. 62, no. 9, pp. 1025–1036, 1996.
- [9] A. Makarau, R. Richter, R. Muller, and P. Reinartz, “Haze detection and removal in remotely sensed multispectral imagery,” *IEEE Transactions on Geoscience and Remote Sensing*, vol. 52, no. 9, pp. 5895–5905, 2014.
- [10] Y. Zhang, B. Guindon, and J. Cihlar, “An image transform to characterize and compensate for spatial variations in thin cloud contamination of Landsat images,” *Remote Sensing of Environment*, vol. 82, no. 2-3, pp. 173–187, 2002.
- [11] W. Ni, X. Gao, and Y. Wang, “Single satellite image dehazing via linear intensity transformation and local property analysis,” *Neurocomputing*, vol. 175, pp. 25–39, 2015.
- [12] Y. Y. Schechner, S. G. Narasimhan, and S. K. Nayar, “Polarization-based vision through haze,” *Applied Optics*, vol. 42, no. 3, pp. 511–525, 2003.
- [13] W. Wang, W. Li, Q. Guan, and M. Qi, “Multiscale single image dehazing based on adaptive wavelet fusion,” *Mathematical Problems in Engineering*, vol. 2015, Article ID 131082, 14 pages, 2015.
- [14] F. Liu, L. Cao, X. Shao, P. Han, and X. Bin, “Polarimetric dehazing utilizing spatial frequency segregation of images,” *Applied Optics*, vol. 54, no. 27, pp. 8116–8122, 2015.
- [15] Y. Li, Q. Miao, R. Liu, J. Song, Y. Quan, and Y. Huang, “A multi-scale fusion scheme based on haze-relevant features for single image dehazing,” *Neurocomputing*, vol. 283, pp. 73–86, 2018.
- [16] W. Ren, S. Liu, H. Zhang, J. Pan, X. Cao, and M.-H. Yang, “Single image dehazing via multi-scale convolutional neural networks,” in *Proceedings of the European Conference on Computer Vision*, pp. 154–169, Springer, Switzerland, 2016.
- [17] B. Li, X. Peng, Z. Wang, J. Xu, and D. Feng, “AOD-Net: All-in-one dehazing network,” in *Proceedings of the 16th IEEE International Conference on Computer Vision, ICCV 2017*, pp. 4780–4788, Italy, October 2017.
- [18] K. Tang, J. Yang, and J. Wang, “Investigating haze-relevant features in a learning framework for image dehazing,” in *Proceedings of the 27th IEEE Conference on Computer Vision and Pattern Recognition (CVPR '14)*, pp. 2995–3002, IEEE, Columbus, Ohio, USA, June 2014.
- [19] B. Jiang, W. Zhang, J. Zhao et al., “Gray-scale image dehazing guided by scene depth information,” *Mathematical Problems in Engineering*, vol. 2016, Article ID 7809214, 10 pages, 2016.
- [20] G. Zhenfei, M. Ju, and D. Zhang, “A single image dehazing method using average saturation prior,” *Mathematical Problems in Engineering*, vol. 2017, Article ID 6851301, 17 pages, 2017.
- [21] R. T. Tan, “Visibility in bad weather from a single image,” in *Proceedings of the 26th IEEE Conference on Computer Vision and Pattern Recognition (CVPR '08)*, pp. 1–8, Anchorage, Alaska, USA, June 2008.
- [22] R. Fattal, *Single Image Dehazing*, ACM, 2008.
- [23] K. He, J. Sun, and X. Tang, “Single image haze removal using dark channel prior,” *IEEE Transactions on Pattern Analysis and Machine Intelligence*, vol. 33, no. 12, pp. 2341–2353, 2011.
- [24] S. K. Nayar and S. G. Narasimhan, “Vision in bad weather,” in *Proceedings of the 7th IEEE International Conference on Computer Vision (ICCV '99)*, vol. 2, pp. 820–827, IEEE, Kerkyra, Greece, September 1999.
- [25] S. G. Narasimhan and S. K. Nayar, “Vision and the atmosphere,” *International Journal of Computer Vision*, vol. 48, no. 3, pp. 233–254, 2002.
- [26] S. Ansia and A. L. Aswathy, “Single image haze removal using white balancing and saliency map,” in *Proceedings of the International Conference on Information and Communication Technologies, ICICT 2014*, pp. 12–19, India, December 2014.
- [27] Q. Zhu, J. Mai, and L. Shao, “A fast single image haze removal algorithm using color attenuation prior,” *IEEE Transactions on Image Processing*, vol. 24, no. 11, pp. 3522–3533, 2015.
- [28] L. I. Changling, Y. Song, and X. Liu, “Haze removal method for traffic images based on multi-scale retinex theory,” *Journal of Computer Applications*, 2015.
- [29] E. Peli, “Contrast in complex images,” *Journal of the Optical Society of America A: Optics and Image Science, and Vision*, vol. 7, no. 10, pp. 2023–2040, 1990.
- [30] Y. Song, H. Luo, R. Lu, and J. Ma, “Dehazed image quality assessment by haze-line theory,” *Journal of Physics Conference Series*, 2017.
- [31] D. J. Jobson, Z.-U. Rahman, G. A. Woodell, and G. D. Hines, “A comparison of visual statistics for the image enhancement of FORESITE aerial images with those of major image classes,” in *Proceedings of the SPIE - The International Society for Optical Engineering*, USA, April 2006.
- [32] L. K. Choi, J. You, and A. C. Bovik, “Referenceless prediction of perceptual fog density and perceptual image defogging,” *IEEE Transactions on Image Processing*, vol. 24, no. 11, pp. 3888–3901, 2015.

